Heliyon 6 (2020) e03620

Contents lists available at ScienceDirect

Heliyon

journal homepage: www.cell.com/heliyon

Research article

Theoretical investigation using DFT of quinoxaline derivatives for electronic and photovoltaic effects

A. El Assyry [a,b,**], M. Lamsayah [c], I. Warad [d], R. Touzani [c], F. Bentiss [e], A. Zarrouk [f,*]

[a] Laboratory of Polymer Physics and Critical Phenomena, University Hassan II, Department of Physics, Faculty of Sciences Ben M'Sik, Casablanca, Morocco
[b] Laboratory of Optoelectronic, Physical Chemistry of Materials and Environment, Department of Physics, Faculty of Sciences, Ibn Tofail University, PB.133, 1400, Kenitra, Morocco
[c] Laboratory of Applied Chemistry and Environment, LCAE, Faculty of Sciences, Mohammed First University, B.P. 717, 60 000, Oujda, Morocco
[d] Department of Chemistry and Earth Sciences, PO Box 2713, Qatar University, Doha, Qatar
[e] Laboratoire de Catalyse et de Corrosion des Matériaux (LCCM), Faculté des Sciences, Université Chouaib Doukkali, BP 20, 24000, El Jadida, Morocco
[f] Laboratory of Materials, Nanotechnology and Environment, Faculty of Sciences, Mohammed V University, Av. Ibn Battouta, P.O. Box 1014, Agdal-Rabat, Morocco

ARTICLE INFO

Keywords:
Energy
Physics
Computing methodology
Theoretical computer science
Molecular physics
Particle physics
Quantum mechanics
TD-DFT
PCM
Quinoxaline derivatives
Solar cells
Optoelectronic
Photovoltaic

ABSTRACT

Photovoltaic properties of solar cells based on fifteen organic dyes have been studied in this work. B3LYP/6-311G (d,p) methods are realized to obtain geometries and optimize the electronic properties, optical and photovoltaic parameters for some quinoxaline derivatives. The results showed that time dependent DFT investigations using the CAM-B3LYP method with the polarized split-valence 6-311G (d,p) basis sets and the polarizable continuum model PCM model were sensibly able to predict the excitation energies, the spectroscopy of the compounds. HOMO and LUMO energy levels of these molecules can make a positive impact on the process of electron injection and dye regeneration. Gaps energy ΔE_g, short-circuit current density J_{sc}, light-harvesting efficiency LHE, injection driving force ΔG^{inject}, total reorganization energy λ_{total} and open-circuit photovoltage V_{oc} enable qualitative predictions about the reactivity of these dyes.

1. Introduction

The quinoxaline derivatives have also found applications in molecules [1, 2, 3, 4, 5, 6, 7, 8]. Newly, the research of synthesis, structural and energetic properties of these compounds were made by our group [9, 10, 11, 12, 13, 14]. In addition, the organic photovoltaic solar cells represent a significant potential for evolution in the study of the electricity production from low-cost compositions. Then, the past 2 years we have seen an important growth in the conversion efficiency of organic photovoltaic solar cell PVSC, pass a 1% return realized in recent years [15], at a 5% recorded in 2 years ago [16]. The long-term goal of this study is to minimize costs of PV compositions; we present here a few technical aspects. There are, to expand a technology founded on eco-friendly materials along nearly limitless availability. This goal becomes achievable day by day, in the evolution of high performance organic screens in the electronic industry [17]. We use the diode technology of organic light-emitting [18] to establish guidelines for organic photovoltaic solar cell OPVCs research. Advances in OPVCs need a distinct agreement of the particular physics of deformed organic semiconductors and devices [19]. We begin by the essential properties of organic semiconductors, as charge transport. We provide guidance for choosing efficient OPV materials and we verify a few castes of materials used in various coats of a PVCs. Then, we present an electrical representation of organic solar cell OSC. A criticism analysis of physical procedures allows us to size the maximum and minimum yields possible using several device structures.

* Corresponding author.
** Corresponding author.
E-mail addresses: abdeslam_elassyry@yahoo.fr (A. El Assyry), azarrouk@gmail.com (A. Zarrouk).

https://doi.org/10.1016/j.heliyon.2020.e03620
Received 24 May 2019; Received in revised form 15 October 2019; Accepted 13 March 2020

Lately, polymer PVCs have received a lot of attention for their flexibility, ease of processing, weak weight and weak cost of production [20, 21, 22]. Their relatively large band gaps limited the J_{sc}, reducing the power conversion efficiencies (PCE). After improving efficiency, low band-gap conjugated polymers (CPs), were developed to better conform to solar spectra, and thus produce higher J_{sc} [23]. Significant advance was done in PVCs founded on bulk-heterojunction networks done of weak band gap CPs and the fullerenes at last, Nowadays the photoelectric conversion efficiency of OSC is much greater than 7% [24]. Generally, the PCE based on the V_{oc}, the J_{sc}, and the fill factor (*FF*) of the systems. The J_{sc} is controlled by the hatching among the absorption of the CPs and the solar spectra [25]. The V_{oc} is calculated by variance among the E_{LUMO} of the fullerene derivatives, and the E_{HOMO} of CPs [26]. So the novel improvement in PCE request development of new CPs with adequate energy levels and greater absorption along the solar spectra. Thus, the mobility of the heavy load carrier of polymer semiconductors should be considered [27].

On the other hand, with the experimental results obtained for organic compounds without metals, research is again restricted. Just some study groups have searched the photophysical and optoelectronic properties for dye sensitizers [28, 29], as well intra compound e^--dynamic process enter compound and TiO_2 [30,31]. So, the investigation study of novel quinoxaline-based dyes was signalized in Figure 1. The central quinoxaline was paired by means of conjugation to an (benzene, chlorobenzene, methylbenzene …) and the group (C=O, $–NO_2$, $–C_3H_5$, …).

The optical absorption and e^--structure properties of fifteen dye sensitizers Q_i (i = 1–15) were investigated by using DFT. According to the results obtained, we analyzed the role of various e^--D groups in setting of structures, optical absorption and e^--structure properties have been analyzed. As well, we wanted to see the sensitizer D impacts on the

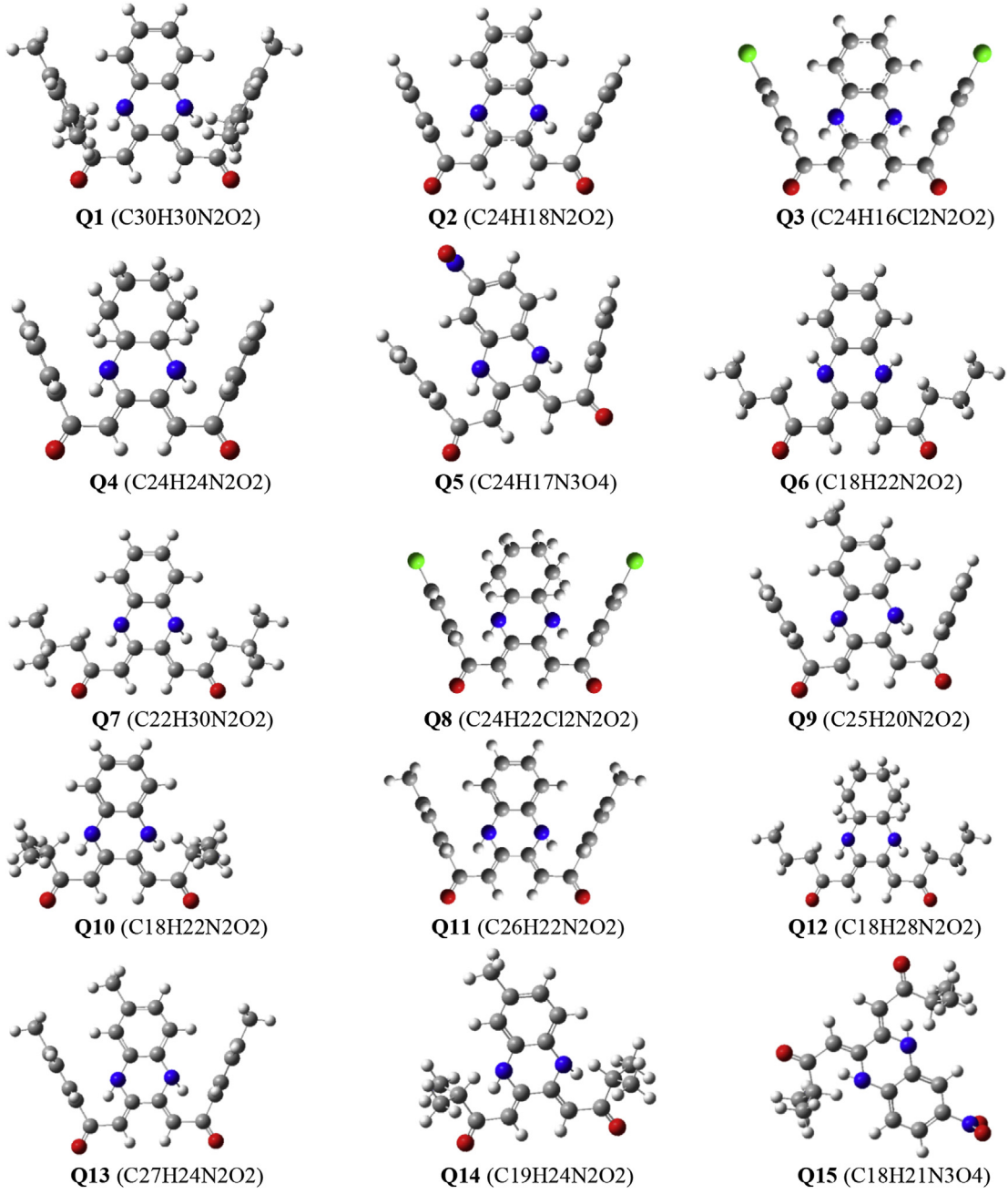

Figure 1. Optimized geometries of all molecules.

V_{oc} and the J_{sc} of the cell via discuss the main factors influencing V_{oc} and J_{sc} along the purpose to discovery the potential sensitizers for use in dye-sensitized solar cell DSSC.

2. Theoretical methodology

2.1. Theoretical background

The design of current–voltage features of a cell below lighting and in darkness, allows evaluating more of its PV performances as well as its electrical behavior [32]. The maximum power P_{max} issued by the PVC; *FF* is defined as:

$$FF = \frac{P_{max}}{V_{oc} \times I_{sc}} = \frac{V_{max} \times I_{max}}{V_{oc} \times I_{sc}}$$

The Incident Photon to Current Efficiency (IPCE) is determined by: [33];

$$IPCE = \frac{J_{sc}}{G \times \lambda} \times \frac{hc}{e}$$

Other: IPCE $= 1.24_{sc}/(G \times \lambda)$

The external PV yield η is described according to the illumination G and the surface S by:

$$\eta = \frac{P_{max}}{S \times G}$$

The conversion yield is very important for cell productivity. This must be carefully estimated [34], and not be abashed with IPCE. The cell drives during the voltage surpass a threshold *Vs*. or I_s is the saturation current in inverse polarization, an ideal cell can follow the thermionic injection model [35]:

$$I = I_s\left(\exp\left(\frac{eV}{kT} - 1\right)\right)$$

For the J_{sc} in DSSC: $J_{sc} = \int_{\lambda} LHE(\lambda)\varphi_{inject}\eta_{collect}d\lambda$

Φ_{inject}: Electron injection efficiency, $\eta_{collect}$: Charge collection efficiency. For the even DSSC by just various molecules, so we can assume that: $\eta_{collect}$ = Constant. Then, to make light on the link enter the J_{sc} and η, we calculated the *LHE*, Φ_{inject} and λ_{total}. For a high J_{sc}, the efficient sensitizers used in DSSC having had to a broad *LHE*, that determined by [36]:

$$LHE = 1 - 10^{-f}$$

where f is the oscillator strength of the dye associate to the λ_{max}. We noticed that the larger oscillator strength would have the higher light-harvesting efficiency. Thus, a large Φ_{inject} could also guarantee a high J_{sc}, who is linked to the ΔG^{inject} and evaluated as [36]:

$$\Delta G^{inject} = E^{dye^*} + E_{CB};\ \text{with}\ E^{dye^*} = E^{dye} - E_{00}$$

where E^{dye} and E^{dye^*} : oxidation potential energy of the composed in the ground and excited state;

E_{CB}: reduction potential of the conduction band of TiO_2.

So, in this study, we use $E_{CB} = -4.0$ eV for TiO_2 [37], that is broadly used in a few works [38, 39, 40], and the E^{dye^*} can be evaluated [39, 40, 41]; and E_{00} is an electronic vertical transition energy associate to λ_{max}. It has in general admitted that there are 2 diagrams to estimate the ΔG^{inject}. Thereby, the e^- injection with excited states of the compound to TiO_2 (CB) is calculated by unrelax path. The small $\lambda_{total,}$ that contains the hole and e^- reorganization energy (λ_h and λ_e) could improve the J_{sc}. Thus, we calculated the (λ_h and λ_e) by [33, 42]:

$$\lambda_i = \left(E_0^{\pm} - E_{\pm}^{\pm}\right) + \left(E_{\pm}^{0} - E_0\right)$$

$E_0^{\pm}$: Cation or anion Energy obtained with the optimized neutral molecule structure,

$E_{\pm}^{\pm}$: Cation or anion Energy obtained with the optimized cation or anion structure,

$E_{\pm}^{0}$: Neutral molecule Energy calculated at the cationic or anionic state,

E_0 : Neutral molecule Energy at ground state.

Figure 2 present the equivalent circuit, who is an absolute current generator. Where I_L is a current source of which intensity according to G, R_s and R_{sh} are the series and shunt resistances; R_L is the charge resistance of the external circuit [35]. The I_{sc} is the one who passes the cell at zero utilized voltage.

The slope near zero polarization is a value of the R_{sh}, who matches to leaks and shorts in the diode [43]. If we assume such: ($R_s = 0$; $R_{sh} = \infty$) with ($I = 0$; $I_L = I_{sc}$), The V_{oc} determined by:

$$V_{oc} = \frac{nkT}{e}\ln\left(\frac{I_{sc}}{I_{sc}} + 1\right)$$

A small R_{sh} will decrease V_{oc}. Furthermore, within the weak illumination G the cell will not be liberated any voltage; I_{sc} decreased by the R_s. The V_{oc} can be calculated by the analytical equation [38]:

$V_{oc} = E_{LUMO} - E_{CB}$

2.2. Calculation methods

Every our investigations have been effected in the gas phase by the DFT optimization with the B3LYP hybrid functional [44, 45, 46] and 6-31G (d,p) Gaussian basis sets [47, 48]. The provide excited state energy and oscillator strength (f) have been calculated using the TD-DFT/CAM-B3LYP methods in chloroform solvent. In this work, the integral equation formalism polarizable continuum model (IEF-PCM) [49, 50, 51, 52] has been selected in excitation energy; while to determinate the λ_{total}, we investigated at the B3LYP/6-311G (d,p) level the cationic and anionic states for each compound.

3. Results and discussion

3.1. Synthesized

We have synthesized these symmetric ligands in good yields, by varying the nature of ortho phenlene diamine substituents. It is carried out in ethanol by two steps: the first step aims to elaborate new tetraone compound. In the second step we condensate the precursor with one equivalent of the 1,2-o-phenylenediamine [53, 54, 55, 56, 57].

3.2. Geometrical structures

In this paper, the quinoxaline dyes [53, 54, 55, 56, 57, 58] chemical structures presented in Figure 1. In other papers, the DFT-investigated geometries have been a good according with the result observed in x-ray analysis [59, 60]. The calculated for every compounds indicate that

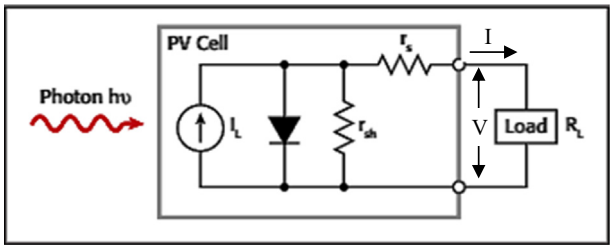

Figure 2. Idealized equivalent circuit of a real PVC under light.

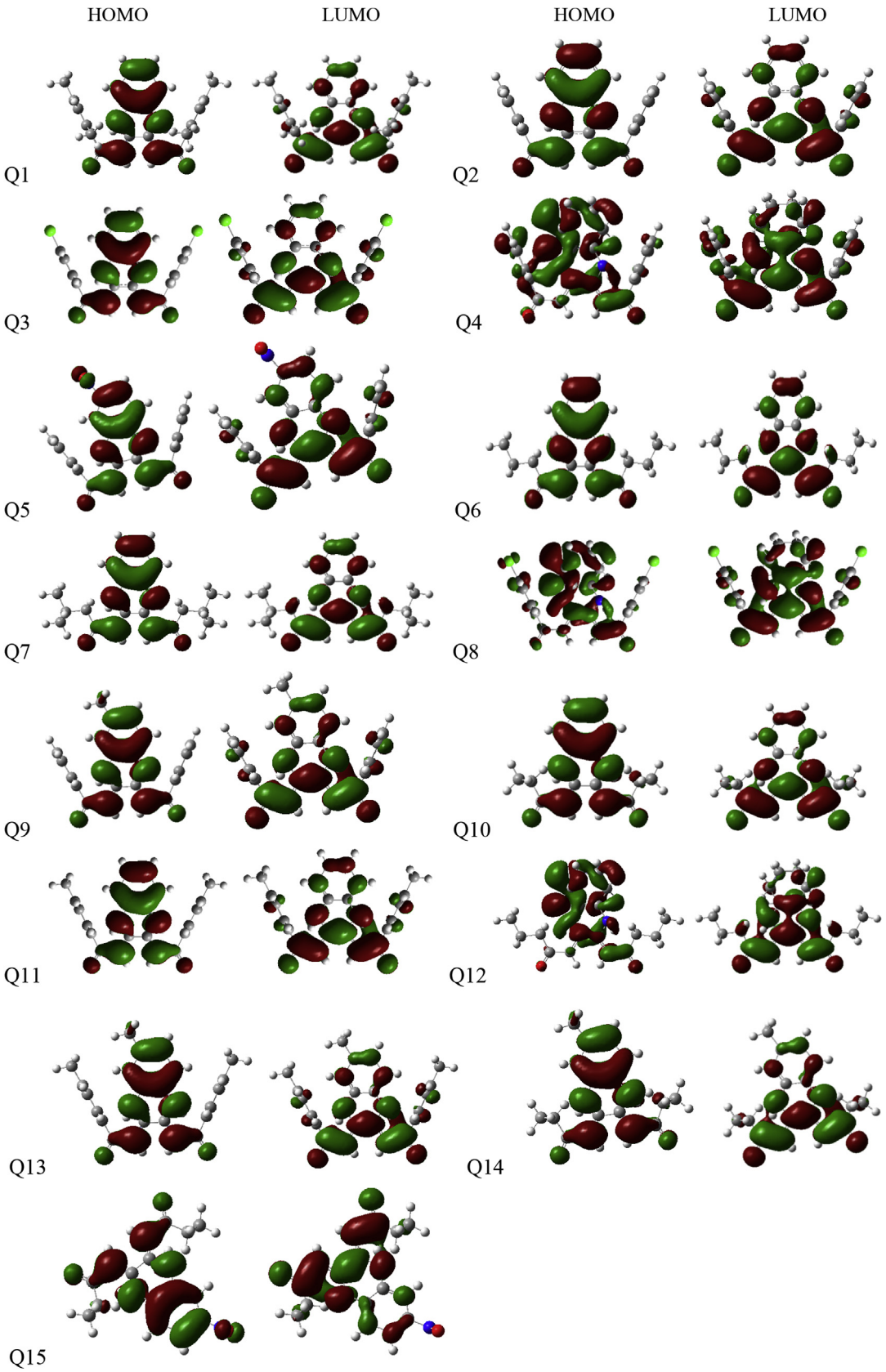

Figure 3. Frontier orbital contour plots of all molecules.

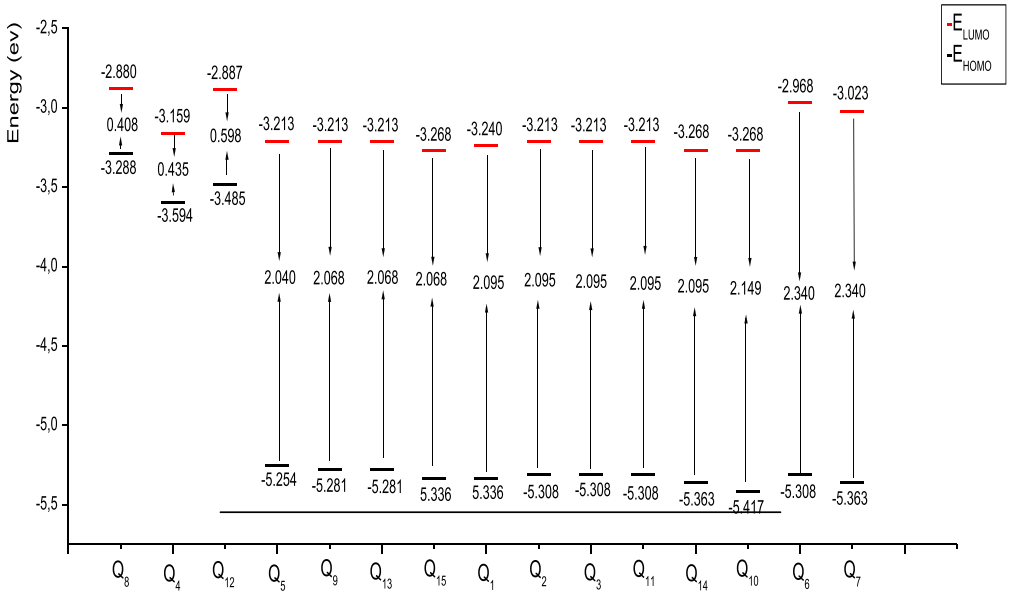

Figure 4. Schematic energy diagram of all molecules.

they have a similar coplanar structure. This coplanar compound-conformation should ameliorate the e^- transfer from the e^--D to the e^--A across the π-spacer unit for our molecules. The optimized critical bond lengths (d_1, d_2) are compared from Q*i* ($i = 1$–15) in ground and excited state (S_0, S_1). The corresponding structural parameters in S_0 are similar to each other. Thus, that both of them, substituent introduction and conjugate chain elongating, have a minor impact on these structural parameters as though the compounds have like π-conjugated linker. That the bond lengths parameters d_1 and d_2 of all molecules is in the range of (1.326 ± 0.03 Å) in S_0, and in S_1 is in the range of (d (S_0) ± 0.018 Å), who is likely due to the conjugation extension. Furthermore, the linkage among the e^--D and π-conjugated bridge is between 1.278–1.374 Å showing in particular more C=C character who favors ICT. Effectively, the π-conjugated group, is used as a deck from ICT of the e^--D to e^--A group. As we know, about to the S_1 photoexcitation, the bond lengths for all compounds notably decreased in similitude along those in S_0, in particular the linkage among the π-conjugated group and the A-half d_2. From this, we conclude who is significant for the absorption spectrum, that linking of A-group and π-bridge (quinoxaline) is critical for the greatly enhanced ICT feature.

3.3. Intramolecular charge transfer

Using the frontier molecular orbital (FMO) we obtain the intramolecular charge transfer (ICT). Figure 3 present the e^- locative distribution of LUMO and HOMO of every molecule. Usually, the parcels of the LUMO and HOMO proved the characteristics π-type MO typical. The HOMO exhibit an anti-bonding type enter two adjacent fragments and bonding type in every unit. The LUMO display the bonding type enter the two adjacent fragments, therefore the lowest lying singlet states are matching to electronic transition of π→π* character. The pattern of LUMOs and HOMOs are similar to each other (Figure 3). The e^- distributions in HOMOs are essentially located in e^--D to π-conjugated spacing, whilst LUMOs are mainly localized on the conjugation spacing half and the e^--A fragments. Thus, the all molecules electronic transitions from HO to LU molecular orbital could lead to ICT from D-units to A/anchoring groups across a conjugated bridge, thus HOMO–LUMO passage maybe ranked as a ππ* ICT. The C=O/anchoring group in all molecules has an important contribution to LUMOs which give a solid electronic coupling with TiO_2 area and thus enhance the e^--injection performance, and thereafter improve the J_{sc}.

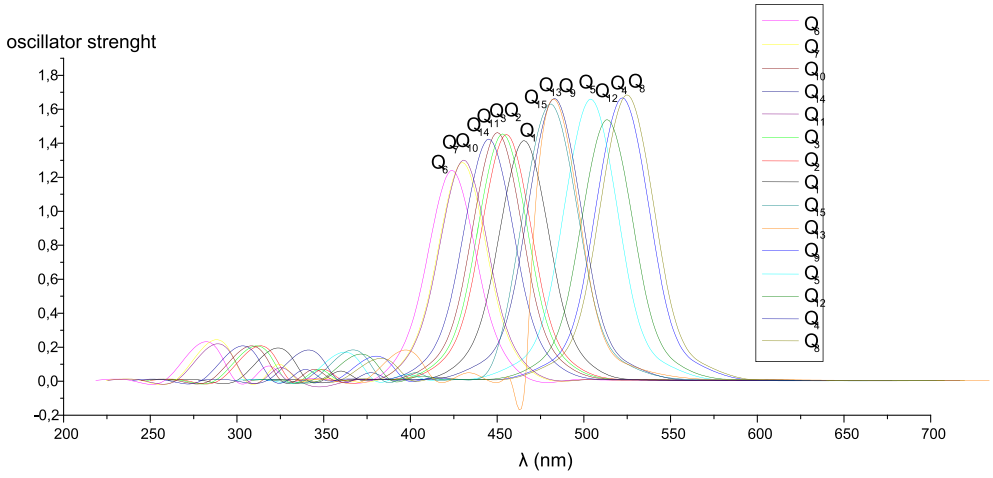

Figure 5. Absorption spectra of all dyes.

Table 1. Emission spectra results for all molecules.

Dye	E_{HOMO} (eV)	E_{LUMO} (eV)	ΔE_g (eV)	E_{00} (eV)	E_{ve} (eV)	λ_{max} (nm)	f	SS (nm)	E_T (eV)	μ (Debye)
Q1	-5.336	-3.240	2.095	2.26	2.70	515.54	1.755	89.3	-38452.23	6.4136
Q2	-5.308	-3.213	2.095	2.25	2.71	505.36	1.752	84.5	-32067.99	6.5906
Q3	-5.308	-3.213	2.095	2.26	2.71	503.17	1.716	80.4	-56960.52	3.3557
Q4	-3.594	-3.159	0.435	0.61	2.41	572.23	1.968	103.8	-32128.91	8.8931
Q5	-5.254	-3.213	2.040	2.10	2.48	553.95	1.960	101.7	-37600.21	2.9054
Q6	-5.308	-2.968	2.340	2.22	2.88	473.92	1.541	57.8	-25949.01	7.8137
Q7	-5.363	-3.023	2.340	2.07	2.85	479.96	1.587	59.7	-30202.29	5.3867
Q8	-3.288	-2.880	0.408	0.33	2.40	575.81	1.994	104.5	-57021.77	5.6837
Q9	-5.281	-3.213	2.068	2.01	2.57	533.07	1.955	99.2	-33132.02	7.0973
Q10	-5.417	-3.268	2.149	2.38	2.84	480.73	1.601	63.1	-25943.16	5.9401
Q11	-5.308	-3.213	2.095	2.29	2.72	500.15	1.709	70.3	-34196.06	7.2559
Q12	-3.485	-2.887	0.598	0.44	2.44	563.40	1.964	95.9	-26007.53	6.6097
Q13	-5.281	-3.213	2.068	2.08	2.61	531.12	1.931	97.5	-35260.09	7.7362
Q14	-5.363	-3.268	2.095	2.37	2.72	495.14	1.703	57.6	-27007.25	6.4986
Q15	-5.336	-3.268	2.068	2.20	2.66	529.05	1.901	96.8	-31475.38	2.2708

3.4. Molecular orbitals

With a stronger e^--D group normally gives a high HOMO as compared to that with a weaker e^--D. Using that, we have calculated the e^--D impact on the electronic properties. Under HOMO, the results of these molecules are:

Q8 > Q12 > Q4 > Q2 = Q3 = Q6 = Q11 > Q5 > Q9 = Q13 > Q15 = Q1 > Q7 = Q14 > Q10. The Q8 marked by the strongest e^--D group (twofold chlorine) as it has the highest HOMO (-3.288 eV). Compounds Q7, Q14 and Q10 with investigating E_{HOMO} respectively -5.363, -5.363 and -5.417 eV, have a low contribution in e^--D capacity because they restrain a group in the e^--donor moiety. The investigated LUMO level in Figure 4 from every sensitizers are comparatively uninfluenced by the modifications in composed geometry, due to the impaction of a few e^--A group (C=O) in these sensitizers, who is less affected by changing of the D-group. The ΔE_g for Qi (i = 1–15) are listed in Figure 4, and the results of ΔE_g is:

Q8 < Q4 < Q12 < Q5 < Q13 = Q15 < Q 1 = Q2 = Q3 = Q11 = Q14 < Q10 < Q7 = Q6. The ΔE_g decrease, another photons at lengthier wavelength side so-called absorbed to excite the e^- until unoccupied MO; that increases the J_{sc} and moreover enhances the conversion efficiency correspondent SC. The ranges of ΔE_g are approximately 0.41–2.34 eV; and therefore, these molecules have the potential employing in the DSSC practice.

3.5. Optical properties

We are getting the optical properties of all sensitized compounds in chloroform solution [61, 62]. The chloroform has been used in UV-Visible absorption spectrum as solvent on quinoxaline based dyes [13, 31]. Since the function used is very economical and requires only one calculation, we took into account for the simulated spectra 20 excited states to obtain a better spectrum for the molecules studied here. The spectrum indicates a similar outline for all molecules; so a principal intense band at highest energies between 300 and 650 nm (Figure 5). The more intense participation to the principal band is an excitation between LUMO and HOMO in solvent as the 1st singlet excitation. Thus, the location (concerning to the gap HOMO-LUMO) and the largeness of 1st band in spectra are the two 1st parameters which can be concerning to compound efficiency, for absorption shift to reduce energies fosters the light harvesting process. The order of 1st vertical excitation energies (E_{ve}) of our molecules is:

Q6 > Q7 > Q10 > Q14 > Q11 > Q3 > Q2 > Q1 > Q15 > Q13 > Q9 > Q5 > Q12 > Q4 > Q8. Therefore, when passing from Q6 to Q8, this shows that there is a bathochromic shift. For Q10, the absorption spectrum of Q7 and Q6 present less decreased oscillator strength with a slight blue shift, due probably to the heteroatom electronegativity in the e^--D groups. The absorption spectrum of Q8, Q4 and Q9 show the main peak at 524.91, 522.23 and 483.07 nm, respectively (Figure 5), which are well shifted to smaller wavelengths relative to those correspondent derivatives. Every data of absorption spectrum are in good, according to the results of band gap and energy debated previously.

The emission spectra in adiabatic measure have been used to study the photoluminescence (PL) characters of the molecules Qi (i = 1–15). We present in Table.1 the investigated fluorescence wavelengths with the strongest oscillator. We obtained the Stokes shift (SS) for all molecules, the emission spectrum arising from the S_1 state is assigned to $\pi^* \rightarrow \pi$ transition and LUMO→HOMO orbital molecule character for all dyes. We establish that the investigated fluorescence emission is only the reverse process of lowest lying absorption. Furthermore, the order of red shift fluorescence observed of PL spectra is:

Q6 < Q7 < Q10 < Q14 < Q11 < Q3 < Q2 < Q1 < Q15 < Q13 < Q9 < Q5 < Q12 < Q4 < Q8; thus the good according with the obtained data of absorption when passing from Q6 to Q8. Moreover, the SS of our molecules has established to be in the range 57.8 and 104.5 nm. The Q8 emitted at higher wavelengths (575.81 nm) with strongest intensity (f = 1.994), and larger SS (104.5 nm). We conclude that Q8 with two fold-chlorine e^--D group will be the best candidate in the DSSC.

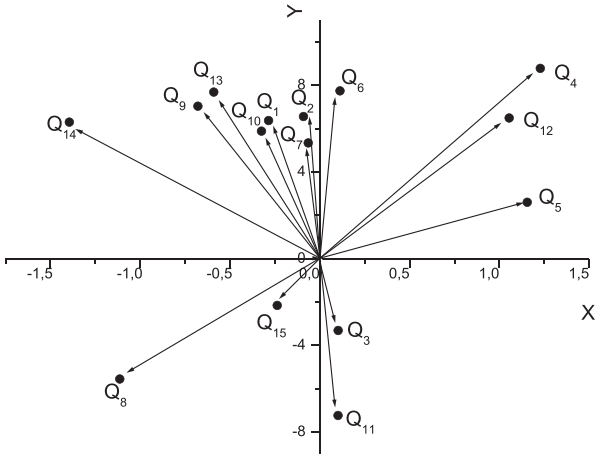

Figure 6. Dipole moments μ (Debye) in a three-dimensional representation, for quinoxalin-2(1H)-one derivatives in Figure 1.

Table 2. Calculated electrochemical parameters for all molecules.

Dye	E^{dye} (eV)	E^{dye*} (eV)	ΔG^{inject} (eV)	LHE	λ_h (eV)	λ_e (eV)	λ_{total} (eV)	V_{oc} (eV)
Q1	5.33	3.07	-0.93	0.9824	0.282	0.321	0.603	0.760
Q2	5.30	3.05	-0.95	0.9822	0.273	0.317	0.590	0.787
Q3	5.30	3.04	-0.96	0.9807	0.280	0.332	0.612	0.787
Q4	3.59	2.98	-1.02	0.9892	0.221	0.280	0.501	0.841
Q5	5.25	3.15	-0.85	0.9890	0.240	0.302	0.542	0.787
Q6	5.30	3.08	-0.92	0.9712	0.263	0.321	0.584	1.032
Q7	5.36	3.29	-0.71	0.9741	0.280	0.352	0.632	0.977
Q8	3.28	2.95	-1.05	0.9898	0.213	0.281	0.494	1.120
Q9	5.28	3.27	-0.73	0.9889	0.270	0.300	0.570	0.787
Q10	5.41	3.03	-0.97	0.9749	0.273	0.331	0.604	0.732
Q11	5.30	3.01	-0.99	0.9804	0.285	0.333	0.618	0.787
Q12	3.48	3.04	-0.96	0.9891	0.241	0.272	0.513	1.113
Q13	5.28	3.20	-0.8	0.9882	0.241	0.323	0.564	0.787
Q14	5.36	2.99	-1.01	0.9801	0.293	0.332	0.625	0.732
Q15	5.33	3.13	-0.87	0.9874	0.231	0.313	0.544	0.732

We presented the dipole moment (μ) vectors in the space of our fifteen quinoxaline molecules (Figure 6). The dipole moment for Q2 (6.590 D) is decreased in (Q1, Q7, Q10) and increased in (Q6, Q9, Q13) with a weak orientation, and even effect has been noted in the compound Q4, Q5, Q12 and Q14 with an orientation important. Furthermore, the μ variations in these ten cases is greatly smaller than that establish in Q3 and Q8 where the existence of electronegative twofold chlorine in the opposite side along respect to carbonyl, not only reduces or increased dramatically the μ, but also modifies the vector orientation along large angle (180° in Q11) (Figure 6). The indication providing by NPA charges as good as this change with account to dipole moment are in according with recognized low eligibility impact of chlorine [46, 50, 63], as likened to its inductive impact.

3.6. Photovoltaic properties

Oxidation potentials energies computed E^{dye} could be optimized as negative E_{HOMO} [64]. E^{dye*} is estimated, E^{dye*} of all molecules is increasing as following:

Q8 < Q4 < Q14 < Q11 < Q10 < Q12 = Q3 < Q2 < Q1 < Q6 < Q15 < Q5 < Q13 < Q9 < Q7. Thus, the most practical oxidizing species is Q8 by

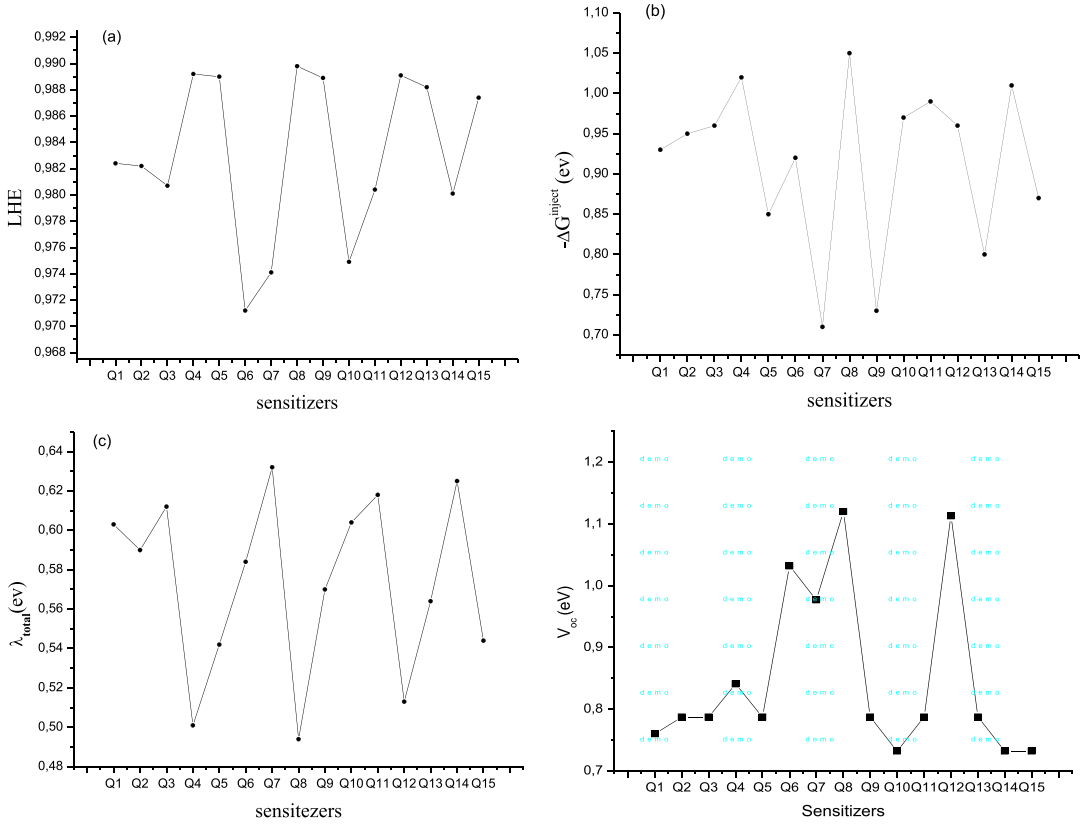

Figure 7. J_{sc} along of calculated sensitizers: (a) the LHE, (b) the ΔG^{inject}, (c) the λ_{total} and (d) the V_{oc}.

cons Q7 is the worst. All ΔG^{inject} obtained is negative for every dyes, so the e^- injection from the composed to TiO_2 is impulsive.

In Table.2 and Figure 6(a) as seen, the estimated ΔG^{inject} are decreased as following:

Q8 > Q4 > Q14 > Q11 > Q10 > Q12 = Q3 > Q2 > Q1 > Q6 > Q15 > Q5 > Q13 > Q9 > Q7. This presents that Q8 has the greatest ΔG^{inject} while Q7 has the littlest value. The result according to LHE of the molecules, must be the highest possible to extend the photocurrent reply. The LHE for every compounds are in close range 0.9712–0.9898, but growth lightly with growthing the conjugation length Figure 7(b); thus which all the dye sensitizers give comparable photocurrent.

In addition to the free energy reaction, the λ_{total} could equally allocate the kinetics of e^- injection. Thus, the investigated λ_{total} is equally significant to analyze the relation among the e^- structure and the critical parameters influenced J_{sc}. Thus, in Table.2 and Figure 7(c) the investigated λ_{total} of all molecules are increased as follows:

Q8 < Q4 < Q12 < Q5 < Q15 < Q13 < Q9 < Q6 < Q2 < Q1 < Q10 < Q3 < Q11 < Q14 < Q7. It shows that composed Q8 possesses the smallest λ_{total}, while composed Q7 has the largest. Consequently, composed Q8 presents a favorable J_{sc} because of the relative similar LHE, larger ΔG^{inject} and smaller λ_{total}. Therefore, ΔG^{inject} and λ_{total} are more important to govern the J_{sc} mostly.

We know that in addition the J_{sc} the overall power conversion efficiency η also could be influenced by the V_{oc}. Thus, between 2 compounds of similar conformations, the e^--injection is more effective for this compound with the higher excited state linked to the semiconductor conduction band edge, that is to say higher V_{oc}. It was found that V_{oc} of all compounds is in the range 0.732–1.120 eV and as following by:

Q8 > Q12 > Q6 > Q7 > Q2 > Q9 > Q4 > Q5 = Q3 = Q2 = Q11 = Q13 > Q1 > Q14 > Q15. It shows that Q8 and Q12 have the higher V_{oc} than other compounds, while Q14 and Q15 have the smallest. Consequently, we conclude that the high (LHE, $-\Delta G^{inject}$ and V_{oc}) and as well small λ_{total} can give an efficiency important. Therefore, the effectiveness of DSSC sensitized by the compound Q8 might be preferable to the other molecules, due to its favorable effectiveness of these factors presented on our calculated results.

4. Conclusions

The results are determined by the DFT investigations using the CAM-B3LYP method.

- The calculated absorption maximums are in the range 473–576 nm;
- The obtained band gap (ΔE_g) of the studied compounds was in the range 0.408–2.340 eV;
- The obtained values of V_{oc} of the studied compounds range from 0.732 to 1.120 eV;
- Since Q8 has the largest value of (LHE, $-\Delta G^{inject}$, V_{oc}) and has the smallest value of (λ_{total}), the compound Q8 was found to be the best photo-sensitizer for use in dye-sensitized solar cell DSSC, in comparison with other dyes, as the investigation results exhibit its good oxidation potential energy and e^- injection force which are above the E_{CB} of TiO_2 and in reduction potential energy of electrolyte.

All the studied compounds can be employed as organic solar cells, because these results are sufficient for an efficient electron injection. To finish, the process of investigated calculations can be used to predict the opto-electronic properties on the other molecules, and more to designing novel materials for organic solar cell.

Declarations

Author contribution statement

A. El Assyry: Conceived and designed the experiments; Performed the experiments; Wrote the paper.

M. Lamsayah: Conceived and designed the experiments; Performed the experiments.

I. Warad & F. Bentiss: Conceived and designed the experiments; Contributed reagents, materials, analysis tools or data.

R. Touzani: Conceived and designed the experiments; Analyzed and interpreted the data.

A. Zarrouk: Analyzed and interpreted the data; Contributed reagents, materials, analysis tools or data; Wrote the paper.

Funding statement

This research did not receive any specific grant from funding agencies in the public, commercial, or not-for-profit sectors.

Competing interest statement

The authors declare no conflict of interest.

Additional information

No additional information is available for this paper.

Acknowledgements

The Hassan II Academy of Science and Technology have supported this work.

References

[1] A. Kumar, S. Kumar, A. Saxena, A. De, S. Mozumdar, Ni-nanoparticles, An efficient catalyst for the synthesis of quinoxalines, Catal. Commun. 9 (5) (2008) 778–7784.
[2] J.Y. Jaung, Synthesis and halochromism of new quinoxaline fluorescent dyes, Dyes Pigm. 71 (3) (2006) 245–250.
[3] K.R.J. Thomas, M. Velusamy, J.T. Lin, C.H. Chuen, Y.T. Tao, Chromophore-labeled quinoxaline derivatives as efficient electroluminescent materials, Chem. Mater. 17 (2005) 1860–1866.
[4] S. Dailey, W.J. Feast, R.J. Peace, I.C. Sage, S. Till, E.L. Wood, Synthesis and device characterisation of side-chain polymer electron transport materials for organic semiconductor applications, J. Mater. Chem. 11 (2001) 2238–2243.
[5] M.J. Crossley, L.A. Johnston, Laterally-extended porphyrin systems incorporating a switchable unit, Chem. Commun. (2002) 1122–1123.
[6] K. Toshima, R. Takano, T. Ozawa, S. Matsumura, Molecular design and evaluation of quinoxaline-carbohydrate hybrids as novel and efficient photo-induced GG-selective DNA cleaving agents, Chem. Commun. 3 (2002) 212–213.
[7] J.L. Sessler, H. Maeda, T. Mizuno, V.M. Lynch, H. Furuta, Quinoxaline-bridged porphyrinoids, J. Am. Chem. Soc. 124 (2002) 13474–13479.
[8] O. Sascha, F. Rudiger, Quinoxalinodehydroannulenes: A novel class of carbon-rich materials, Synlett 15 (2004) 1509–1512.
[9] A. El Assyry, B. Benali, B. Lakhrissi, M. El Faydy, M. Ebn Touhami, R. Touir, M. Touil, Experimental and theoretical comparatives investigation of mild steel corrosion inhibition by quinoxalinone derivatives in 1 M HCl, Res. Chem. Intermed. 41 (2015) 3419–3431.
[10] F. Benhiba, Y. ELaoufir, M. Belayachi, H. Zarrok, A. El Assyry, A. Zarrouk, B. Hammouti, E.E. Ebenso, A. Guenbour, S.S. Al Deyab, H. Oudda, Theoretical and experimental studies on the inhibition of 1,1'-(2- phenylquinoxaline-1,4-diyl) diethanone for the corrosion of carbon steel in 1.0 M HCl, Der Pharm. Lett. 6 (2014) 306–318.
[11] M. Larouj, Y. ELaoufir, H. Serrar, A. El Assyry, M. Galai, A. Zarrouk, B. Hammouti, A. Guenbour, A. El Midaoui, S. Boukhriss, M. Ebn Touhami, H. Oudda, Inhibition effects and theoretical studies of novel synthesized pyrimidothiazine derivative as corrosion inhibitor for carbon steel in phosphoric acid solution, Der Pharm. Lett. 6 (2014) 324–334.
[12] A. El Assyry, B. Benali, A. Boucetta, B. Lakhrissi, Application of the AMYR calculating method on quinoxaline, 3-chloroquinoxaline, and 3-methylquinoxaline in the interaction with n water molecules (n varies from 1 to 6), J. Struct. Chem. 55 (2014) 38–44.
[13] B. Benali, Z. Lazar, A. Boucetta, A. El assyry, B. Lakhrissi, M. Massoui, C. Jermoumi, D. Mondieig, Characterization and spectral study of 1,4-dimethylquinoxaline-2,3-dione potassium iodide complex, Spectr. Lett. 41 (2008) 64–71.
[14] A. El Assyry, B. Benali, R. Jdaa, B. Lakhrissi, M. Touil, A. Zarrouk, Theoretical investigation using AMYR calculations of five quinoxalinones in interaction with water molecules, J. Mater. Environ. Sci. 5 (2014) 1434–1441.
[15] C.W. Tang, Two-layer organic photovoltaic cell, Appl. Phys. Lett. 48 (1986) 183–185.
[16] J.H. Schön, Ch. Kloc, B. Batlogg, Efficient photovoltaic energy conversion in pentacene-based heterojunctions, Appl. Phys. Lett. 77 (2000) 2473–2475.

[17] P. Le Barny, V. Dentan, H. Facoetti, M. Vergnolle, G. Vériot, B. Servet, D. Pribat, Application of organic electroluminescent materials in visualisation, C. R. Acad., Sci. Paris Sér. IV 1 (2000) 493–508.
[18] J. Kalinowski, Electroluminescence in organics, J. Phys. D 32 (1999) R179.
[19] J. Simon, J.-J. André, Molecular Semiconductors: Photoelectrical Properties and Solar Cells, Springer, 1985.
[20] F.C. Krebs, S.A. Gevorgyan, J. Alstrup, A roll-to-roll process to flexible polymer solar cells: model studies, manufacture and operational stability studies, J. Mater. Chem. 19 (2009) 5442–5451.
[21] F.C. Krebs, J. Fyenbo, M. Jørgensen, Product integration of compact roll-to-roll processed polymer solar cell modules: methods and manufacture using flexographic printing, slot-die coating and rotary screen printing, J. Mater. Chem. 20 (2010) 8994–9001.
[22] G. Li, C.-W. Chu, V. Shrotriya, J. Huang, Y. Yang, Efficient inverted polymer solar cells, Appl. Phys. Lett. 88 (2006) 253503.
[23] W.L. Ma, C.Y. Yang, X. Gong, K. Lee, A.J. Heeger, Thermally stable, efficient polymer solar cells with nanoscale control of the interpenetrating network morphology, Adv. Funct. Mater. 15 (2005) 1617–1622.
[24] Y.Y. Liang, Z. Xu, J.B. Xia, S.T. Tsai, Y. Wu, G. Li, C. Ray, L.P. Yu, For the bright future—bulk heterojunction polymer solar cells with power conversion efficiency of 7.4%, Adv. Mater. 22 (2010) E135–E138.
[25] K.L. Mutolo, E.I. Mayo, B.P. Rand, S.R. Forrest, M.E. Thompson, Enhanced open-circuit voltage in subphthalocyanine/C60 organic photovoltaic cells, J. Am. Chem. Soc. 128 (2006) 8108–8109.
[26] A. Gadisa, M. Svensson, M.R. Andersson, O. Inganєas, Correlation between oxidation potential and open-circuit voltage of composite solar cells based on blends of polythiophenes/fullerene derivative, Appl. Phys. Lett. 84 (2004) 1609–1611.
[27] S.H. Chan, C.P. Chen, T.C. Chao, C. Ting, C.S. Lin, B.T. Ko, Synthesis, characterization, and photovoltaic properties of novel semiconducting polymers with Thiophene−Phenylene−Thiophene (TPT) as coplanar units, Macromolecules 41 (2008) 5519–5526.
[28] A. El Assyry, A. Hallaoui, F. Abrighach, R. Touzani, A. Zarrouk, A. Lamhamdi, DFT spectroscopy properties of new N-heterocyclic compounds designed for efficient photovoltaic applications, Der Pharm. Lett. 7 (9) (2015) 151–160.
[29] H.-.X. Ji, Z.-.S. Huang, L. Wang, D. Cao, Quinoxaline-based organic dyes for efficient dye-sensitized solar cells: Effect of different electron-withdrawing auxiliary acceptors on the solar cell performance, Dyes Pigm. 159 (2018) 8–17.
[30] A. El Assyry, R. Jdaa, B. Benali, M. Addou, A. Zarrouk, Optical and photovoltaic properties of new quinoxalin-2(1H)-one-based D-A organic dyes for efficient dye-sensitized solar cell using DFT, J. Mater. Environ. Sci. 6 (2015) 2612–2623.
[31] A. Dessì, G.B. Consiglio, M. Calamante, G. Reginato, A. Mordini, M. Peruzzini, M. Taddei, A. Sinicropi, M.L. Parisi, F.F. Biani, R. Basosi, R. Mori, M. Spatola, M. Bruzzi, L. Zani, Organic chromophores based on a fused bis-thiazole core and their application in dye-sensitized solar cells, Eur. J. Org. Chem. 2013 (2013) 1916–1928.
[32] L. Sicot, C. Fiorini, A. Lorin, P. Raimond, C. Sentein, J.M. Nunzi, Improvement of the photovoltaic properties of polythiophene-based cells, Sol. Energy Mater Sol. Cells 63 (2000) 49–60.
[33] J.-M. Nunzi, Organic photovoltaic materials and devices, C. R. Physique 3 (2002) 523–542.
[34] J. Rostalski, D. Meissner, Monochromatic versus solar efficiencies of organic solar cells, solar energy mater, Solar Cells 61 (2000) 87–95.
[35] S.M. Sze, Physics of Semiconductor Devices, Wiley, 1981.
[36] Z.L. Zhang, L.Y. Zou, A.M. Ren, Y.F. Liu, J.K. Feng, C.C. Sun, Theoretical studies on the electronic structures and optical properties of star-shaped triazatruxene/heterofluorene co-polymers, Dyes Pigm. 96 (2013) 349–363.
[37] J.B. Asbury, Y.Q. Wang, E. Hao, H. Ghosh, T. Lian, Evidences of hot excited state electron injection from sensitizer molecules to TiO2 nanocrystalline thin films, Res. Chem. Intermed. 27 (2001) 393–406.
[38] J. Zhang, H.B. Li, S.L. Sun, Y. Geng, Y. Wu, Z.M. Su, Density functional theory characterization and design of high-performance diarylamine-fluorenedyes with different π spacers for dye-sensitized solar cells, J. Mater. Chem. 22 (2012) 568–576.
[39] A. El Assyry, A. Hallaoui, A. Zarrouk, M. El Hezzat, M. Assouag, S. Boukhris, M.M. Ebn Touhami, DFT investigations on optoelectronic properties of new low gap compounds based on pyran as solar cells materials, Der. Pharma. Chem. 7 (10) (2015) 128–138.
[40] W.L. Ding, D.M. Wang, Z.Y. Geng, X.L. Zhao, W.B. Xu, Density functional theory characterization and verification of high-performance indoline dyes with D–A–π–A architecture for dye-sensitized solar cells, Dyes Pigm. 98 (2013) 125–135.
[41] W. Sang-aroon, S. Saekow, V. Amornkitbamrung, Density functional theory study on the electronic structure of Monascus dyes as photosensitizer for dye-sensitized solar cells, J. Photochem. Photobiol. A. 236 (2012) 35–40.
[42] M.P. Balanay, D.H. Kim, Structures and excitation energies of Zn–tetraarylporphyrin analogues: A theoretical study, J. Mol. Struct. (THEOCHEM) 910 (2009) 20–26.
[43] A. Ricaud, Photopiles solaires, Presses polytechniques et universitaires romandes, 1997.
[44] A.D. Becke, Density-functional thermochemistry. III. The role of exact exchange, J. Chem. Phys. 98 (1993) 5648–5652.
[45] A. El Assyry, A. Hallaoui, R. Saddik, N. Benchat, B. Benali, A. Zarrouk, Gaussian electronic properties studies of organic materials based on pyridazine for efficient photovoltaic devices, Der Pharm. Lett. 7 (9) (2015) 295–304.
[46] A. El Assyry, B. Benali, A. Boucetta, B. Lakhrissi, Quantum chemical study by density functional theory (DFT) of some benzodiazepine derivatives, J. Mater. Environ. Sci. 5 (2014) 1860–1867.
[47] R.J. Magyar, S. Tretiak, Dependence of spurious charge-transfer excited states on orbital exchange in TDDFT: large molecules and clusters, J. Chem. Theory. Comput. 3 (2007) 976–987.
[48] M.J. Frisch, G.W. Trucks, H.B. Schlegel, G.E. Scuseria, M.A. Robb, J.R. Cheeseman, et al., Gaussian 09, revision A.02, Gaussian, Inc., Pittsburgh, PA, 2009.
[49] J. Tomasi, B. Mennucci, R. Cammi, Quantum mechanical continuum solvation models, Chem. Rev. 105 (2005) 2999–3094.
[50] A. El Assyry, B. Benali, A. Boucetta, D. Mondieig, Theoretical investigation of the Cl and CH3 substitutions effect on structural and energy behavior of benzodiazepine, Res. Chem. Intermed. 40 (2014) 1043–1052.
[51] M. Cossi, V. Barone, Time-dependent density functional theory for molecules in liquid solutions, J. Chem. Phys. 115 (2001) 4708–4717.
[52] C. Adamo, V. Barone, A TDDFT study of the electronic spectrum of s-tetrazine in the gas-phase and in aqueous solution, Chem. Phys. Lett. 330 (2000) 152–160.
[53] R. Touzani, T. Ben-Hadda, S. El Kadiri, A. Ramdani, O. Maury, H. Le Bozec, L. Toupet, P.H. Dixneuf, Solution, solid state structure and fluorescence studies of 2,3-functionalized quinoxalines: evidence for a π-delocalized keto-enamine form with N–H···O intramolecular hydrogen bonds, New, J. Chem. 25 (3) (2001) 391–395.
[54] M.J. Waring, T. Ben-Hadda, A.T. Kotchevar, A. Ramdani, R. Touzani, S. Elkadiri, A. Hakkou, M. Bouakka, T. Ellis, 2,3-bifunctionalized quinoxalines: synthesis, DNA interactions and evaluation of anticancer, anti-tuberculosis and antifungal activity, Molecules 7 (8) (2002) 641–656.
[55] I. Bouabdallah, I. Zidane, R. Touzani, B. Hacht, A. Ramdani, Quinoxalines and tetraketones for metal cations extractio, ARKIVOC 10 (2006) 77–81.
[56] T. Xiao, Z.-.S. Huang, L. Wang, D. Cao, Impact of π-spacers of dithieno[3,2-f:2′,3′-h] quinoxaline-based organic dyes with three π-spacers on the solar cell performance, J. Mater. Sci. Mater. Electron. 30 (2018) 647–657.
[57] M. Benabdellah, K. Tabji, B. Hammouti, R. Touzani, A. Aouniti, A. Dafali, S. El Kadiri, He effect of temperature on the corrosion of steel in 1M HCl in the presence of quinoxaline compound, Phys. Chem. News 43 (2008) 115–120.
[58] M. Lamsayah, A. Takfaoui, A. Mouadili, M. Haibach, A.J. Nawara-Hultzsch, T.J. Emge, R. Touzani, Pyrazole and quinoxaline: synthesis and X-ray structural characterization of new tridentate (N,N,N) and bidentate (N,N or N,O) ligands, Mor. J. Chem. 2 (3) (2014) 199–210.
[59] D. Mondieig, Ph. Negrier, J.M. Leger, L. Lakhrissi, A. El Assyry, B. Lakhrissi, E.M. Essassi, B. Benali, A. Boucetta, Synthesis and structural study of N-isopropenylbenzimidazolone, Russ. J. Phys. Chem. A 89 (2015) 807–811.
[60] Ph. Négrier, D. Mondieig, J.M. Léger, B. Benali, Z. Lazar, A. Boucetta, A. Elassyry, B. Lakhrissi, C. Jermoumi, M. Massoui, Crystal structure of benzodiazepin-2,4-dione, Anal. Sci. 22 (2006) 175–176.
[61] D. Jacquemin, E.A. Perpete, I. Ciofinil, C. Adamo, Accurate Simulation of Optical Properties in Dyes, Acc. Chem. Res. 42 (2009) 326–334.
[62] C. Adamo, D. Jacquemin, The calculations of excited-state properties with Time-Dependent Density Functional Theory, Chem. Soc. Rev. 42 (2013) 845–856.
[63] A. El Assyry, B. Benali, Theoretical study of the interaction between benzodiazepine derivatives and water by use of AMYR calculations, Res. Chem. Intermed. 40 (2014) 627–636.
[64] R.G. Pearson, Absolute electronegativity and hardness: application to inorganic chemistry, Inorg. Chem. 27 (1988) 734–740.